Machine learning approach to railway ballast degradation prognosis considering crumb rubber modification and parent rock strength

Koohmishi, Mehdi; Guo, Yunlong

DOI
10.1016/j.conbuildmat.2023.133985

Publication date
2023

Document Version
Final published version

Published in
Construction and Building Materials

Citation (APA)
Koohmishi, M., & Guo, Y. (2023). Machine learning approach to railway ballast degradation prognosis considering crumb rubber modification and parent rock strength. *Construction and Building Materials*, *409*, Article 133985. https://doi.org/10.1016/j.conbuildmat.2023.133985

Construction and Building Materials 409 (2023) 133985

Contents lists available at ScienceDirect

Construction and Building Materials

journal homepage: www.elsevier.com/locate/conbuildmat

Machine learning approach to railway ballast degradation prognosis considering crumb rubber modification and parent rock strength

Mehdi Koohmishi [a,*], Yunlong Guo [b,*]

[a] Department of Civil Engineering, Faculty of Engineering, University of Bojnord, Bojnord, Iran
[b] Faculty of Civil Engineering and Geosciences, Delft University of Technology, Delft 2628CN, Netherlands

ARTICLE INFO

Keywords:
Ballast degradation
Crumb rubber
Parent rock
Impact loading
Random forest
Support vector regression
Machine learning

ABSTRACT

Parent rock strength and crumb rubber modification are two critical mechanical parameters that significantly decide the ballast layer degradation subjected to train dynamic loading. Using machine learning to predict ballast degradation considering these two parameters is helpful for deciding ballasted track maintenance cycle. In the current study, the ballast degradation process data (variables: parent rock types, loading types, ballast gradations and compositions of crumb rubber-ballast mixture) were used to train machine learning models. The drop-weight impact loading tests were performed to simulate different train dynamic loadings.

Two well-established machine learning models, i.e., random forest (RF) and support vector regression (SVR) were trained and verified, to more effectively assess the importance of these variables. The results from the validated machine learning models confirm that the parent rock type is the most influential parameter, followed by the loading type (applied stress level), to control and predict the degradation of the ballast-CR mixture.

The experimental assessment reveals that although the incorporation of CR suppresses degradation across all characterized rock types, the improvement in performance of the ballast-CR specimen against degradation is more noticeable for high-strength parent rock subjected to a considerable stress level. Meanwhile, this positive influence is also observed for ballast of weaker strength when the applied stress level is low.

1. Introduction

The ballast layer is characterized as one of the major components of typical railway ballasted tracks. Comprising large-sized, tough, crushed particles, it serves as a structural layer designed to fulfill the following main functions [18,37,15]:

- Providing stable support for both rails and sleepers subjected to moving train loads,
- Distributing the exerted train forces to reduce the applied pressures on the subgrade,
- Facilitating the process of vertical and lateral adjustment of the track with respect to the geometry and stiffness,
- Draining infiltrated water through the granular system, while also absorbing noise and vibration.

Ballasted track geometry deterioration typically results from ballast layer degradation leading to considerable reduction of lateral stability of track [33]. The degradation of the ballast layer is often attributed to fracture/breakage, wear/abrasion, and the movement of individual ballast particles [15,30]. Factors that influence ballast layer degradation include the types of loading, parent rock type, and the application of geo-inclusions (e.g., crumb rubber/tire-derived aggregates, under-sleeper pads, geogrid, etc.).

Regarding loading types, the train-induced impact loading is absorbed by particle breakage, which wears the angularity and rough surface of ballast particles [35]. In this context, Koohmishi and Palassi [25] assessed the breakage of single ballast particles by performing a point load test (PLT) on individual particles, considering the effects of size and shape. Although the influence of shape was marginal, the size of individual particles was a significant factor. Similarly, Koohmishi [27] conducted a PLT on ballast particles, establishing a bilateral loading condition. As expected, this modified loading approach led to an extension in the point load strength index.

Concerning parent rock type, high-quality igneous or metamorphic rocks are preferred for producing ballast particles to ensure the performance of ballasted tracks. Notably, the parent rock determines the ballast's resistance to weathering, loading, etc. In this respect, Sadeghi

* Corresponding authors.
E-mail addresses: m.koohmishi@ub.ac.ir (M. Koohmishi), yunlong.guo@tudelft.nl (Y. Guo).

https://doi.org/10.1016/j.conbuildmat.2023.133985
Received 25 July 2023; Received in revised form 16 October 2023; Accepted 25 October 2023
Available online 31 October 2023

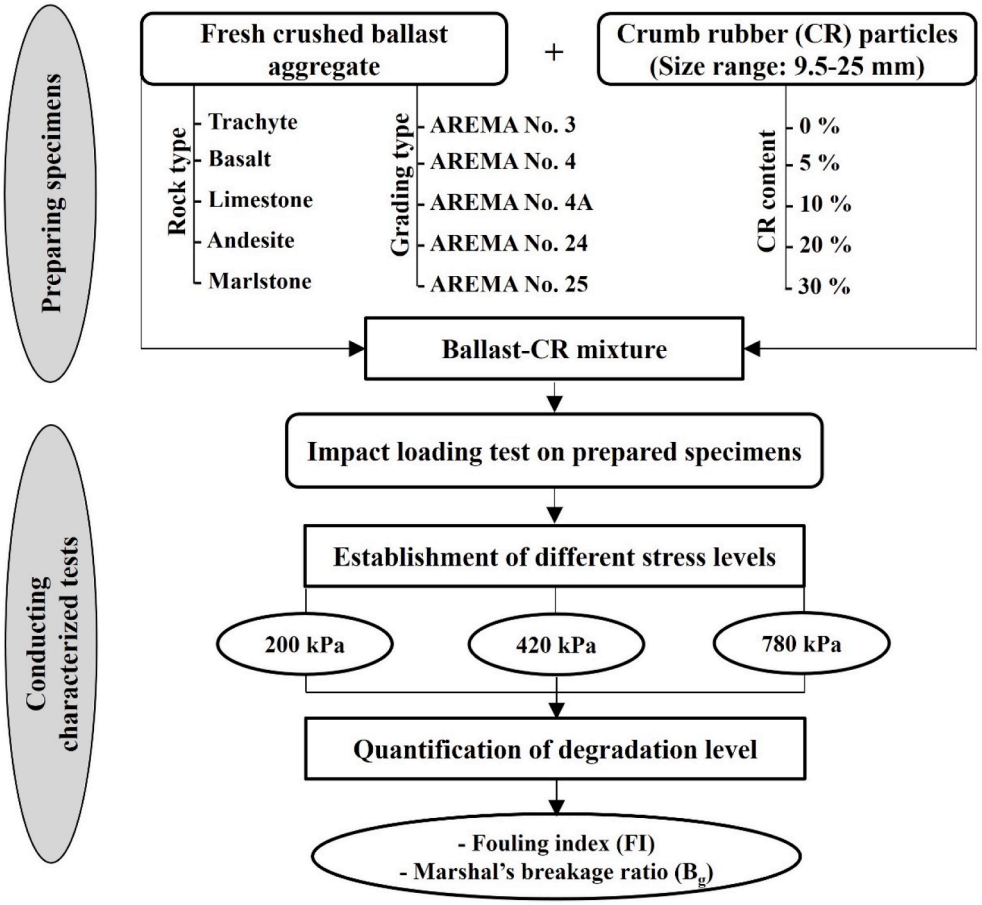

a Characterized conditions for carrying out the large-scale impact loading test on ballast reinforced with CR particles

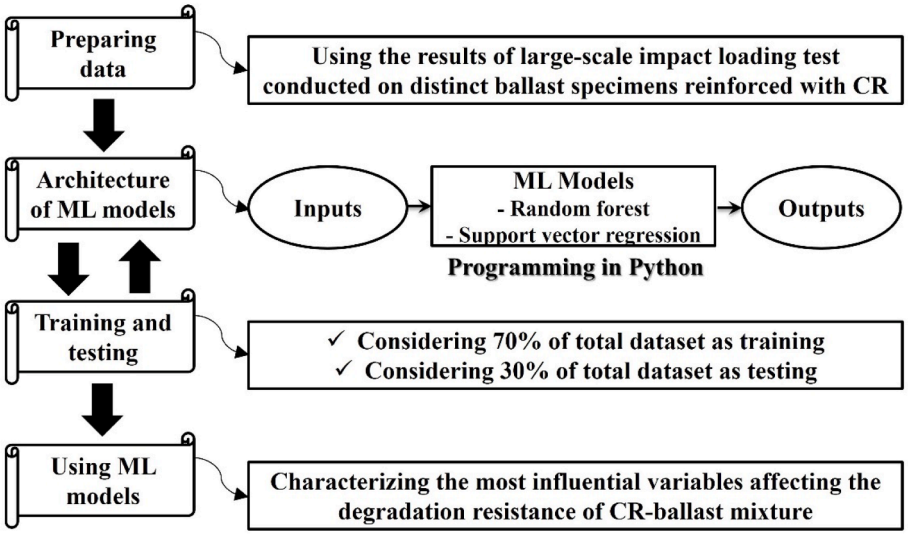

b Development of ML models

Fig. 1. Flowchart representing the process of sequential divisions being followed in the current study. a Characterized conditions for carrying out the large-scale impact loading test on ballast reinforced with CR particles. b Development of ML models.

Table 1
General properties of rock-type ballast derived from distinct queries in Iran.

Rock type	Color	PLSI[1] (MPa)	Water absorption[2] (%)	LAAI[3] (%)
Trachyte	Grayish yellow	13.4	1.73	14.6
Basalt	Gray	11.9	0.56	18.5
Limestone	Light grayish white	10.8	0.55	22.6
Andesite	Dark purple	9.2	0.39	23.0
Marlstone	Grayish white	5.9	0.32	29.5

[1] Average value of point load strength index of cube-shaped individual particle - Sieve size range of 37.5–50 mm [6].
[2] ASTM C 127-12 [8].
[3] Los Angeles abrasion index [7].

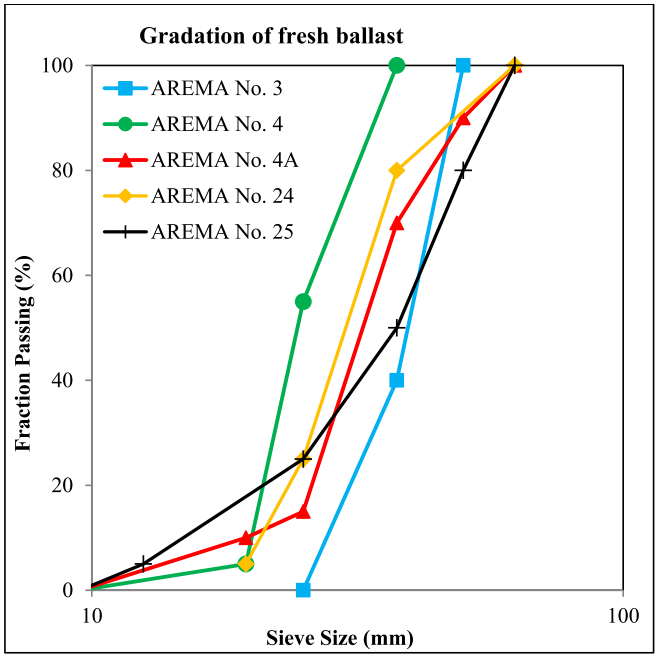

Fig. 2. Gradation curves of ballast particles considered in the current study.

Table 2
Main characteristics relevant to the characterized gradations of fresh crushed ballast particles.

Grading type	d_{max} (mm)	d_{min} (mm)	d_{10} (mm)	d_{60} (mm)	C_u
AREMA No. 3	50	25	28.1	41.2	1.47
AREMA No. 4	37.5	9.5	20.1	26.4	1.31
AREMA No. 4A	62.5	9.5	19.5	35.2	1.81
AREMA No. 24	62.5	25	28.1	45.5	1.62
AREMA No. 25	62.5	4.75	15.0	41.3	2.75

et al. [37] categorized the parent rock for the selection of ballast into four subdivisions: igneous, metamorphic, sedimentary rocks, and slag aggregate. Similarly, Alabbasi and Hussein [2] noted that the most widely used parent rock for the ballast layer of railway tracks is extrusive igneous rocks, followed by metamorphic and then sedimentary rocks. Given the importance of the strength of the parent rock, as reported by Wnek et al. [46], the geological characteristics and the quarrying process were crucial factors influencing the mechanical and physical properties of crushed stone ballast.

As for geo-inclusions, various practical methods have been employed to mitigate ballast layer degradation in ballasted tracks. These include the placement of under-sleeper pads and under-ballast mats, as well as the incorporation of crumb rubber (CR) into the ballast layer. Mixing crumb rubber with ballast could be an effective solution due to the disposal of waste tires and the associated reduction in vibration of the ballast layer. Truly, appropriate reusing of these solid wastes can reduce environmental burdens [22,23]. In relation to this, Sol-Sánchez et al. [39] conducted a cyclic uniaxial compression test on ballast-CR samples and concluded that the fusion of CR particles abated both degradation and stiffness. Similarly, establishing the stone-rubber blowing minimized the recurrence of track maintenance due to degradation reduction [40]. Sol-Sánchez et al. [41] discovered that adding rubber particles could provide an elastic layer beneath the sleepers.

Considering the influence of size and quantity of CR particles, Guo et al. [13] assessed the degradation reduction of ballast-crumb rubber specimens by implementing the Los Angeles Abrasion (LAA) test. They found that incorporating larger-sized CR, comparable to the size of ballast, led to a lower impact on degradation mitigation [13]. Likewise, Koohmishi and Azarhosh (2021) conducted a drop-weight impact loading test on mixtures of crushed basalt ballast and CR particles, considering the influence of the content and size of rubber material. Moreover, Zhang et al. [48] assessed the influence of CR on corner abrasion and bulk fracture of ballast particles subjected to impact loading. The results confirmed that the most significant effect was achieved in the size range of 25–35.5 mm. Furthermore, Arachchige et al. [4] proposed a design criterion in which the acceptable range of weight percentages of rubber was concluded to be between 7.5 % and 10 %, considering the compound effects of breakage and associated axial strain. Establishing the numerical analysis, Guo et al. [16] concluded that smaller-sized CR particles had a more significant influence on the dynamic interaction of the train-track-subgrade system. Zhang et al. [49] simulated the box test by developing a discrete element model in PFC3D. The observed results supported a more homogeneous distribution of contact forces when a higher percentage of CR was incorporated, leading to a reduction in the possibility of particle breakage.

Taking into account the influence of parent rock, Esmaeili and Namaei [11] conducted a ballast box test on rubber-coated ballast (RCB) specimens. The test results corroborated that softer ballast resulted in the most substantial improvement of RCB deterioration, even though the level of stiffness reduction was independent of the parent rock type. Similarly, Esmaeili et al. [12] categorized ballast materials based on the uniaxial compressive strength (UCS) into hard rock core and considerably hard rock core to scrutinize the influence of rock strength on the degradation degree of ballast particles equipped with under-sleeper mats. Recently, approaches based on the artificial intelligence, such as machine learning (ML), are characterized as well-established methods to predict the considered target feature. However, until now machine learning to ballast degradation prognosis considering crumb rubber modification and parent rock strength has never been performed.

Multiple earlier studies have revealed the achievability of machine learning employment for predicting railway ballast performance. Liu et al. [29] employed artificial neural networks (ANN), support vector machines (SVM), random forests (RF), and multiple linear regression to envision the rut depth of asphalt concrete. Zhang et al. [50] assessed the potency of distinct machine learning methods for predicting the compressive strength of cement-reinforced soil. Regarding the usage of machine learning models in ballasted railway tracks, Aela et al. [1] used machine learning methods to predict the number and sizes of ballast granular particles after breakage, considering three distinct types of ballast material. Statistical indices identified RF regression as the best method for estimating the size of crushed particles.

Azarhoosh and Koohmishi [9] utilized distinct models, including adaptive network-based fuzzy inference systems (ANFIS), ANNs, and RFs, to predict the hydraulic conductivity of large-sized particles, such as railway ballast. The comparative analysis revealed RF as the most appropriate approach. Similarly, Indraratna et al. [19] employed ANFIS and ANNs to predict the resilient modulus of ballast subjected to cyclic loading.

A thorough literature review confirms that the effect of combining CR with ballast on particle degradation resistance has been extensively

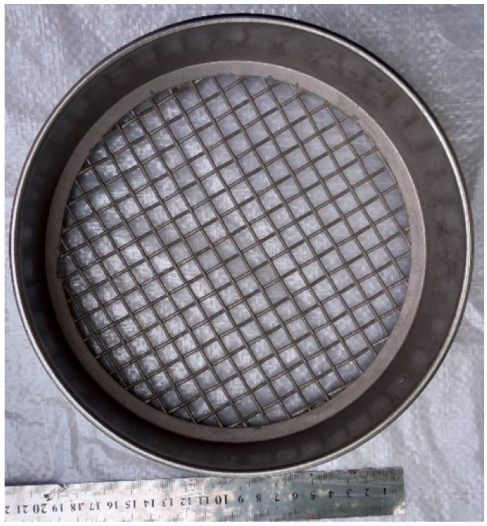

a CR - Size range: 9.5-25 mm

Basalt Limestone Andesite

b.1 CR content: 0%

Fig. 3. Prepared mixtures of ballast-rubber particles.

Basalt Limestone Andesite

b.2 CR content: 5%

Basalt Limestone Andesite

b.3 CR content: 20%

b Distinct mixtures of ballast and CR

Fig. 3. (*continued*).

addressed in previous research. The determination of the optimal percentage of rubber material and the appropriate size range for the most positive effect of rubber granules on ballast degradation resistance were all evaluated in preceding investigations [13,26,16,48]. However, the contribution of the strength of the parent rock for ballast particles reinforced with granulated rubber particles is not clear. Moreover, there is no study in which the effects of distinct parameters, including the parent rock, the gradation of ballast, the applied stress level, and the CR content, have been thoroughly considered. Most importantly, no studies have been performed using machine learning to predict ballast degradation considering these parameters.

To address these research gaps, a series of drop-weight impact loading tests were performed to establish the dataset. Based on the prepared dataset, consisting of 360 specimens, we established high-powered machine learning methods to predict ballast degradation, considering the parent rock, gradation of ballast, crumb rubber reinforcement, and loading conditions. These influential variables significantly affect the degradation resistance of ballast particles. The results reveal the most critical variable, along with the individual effect of each characterized condition. The research output is very helpful for the smart maintenance of railway ballasted tracks by providing a more precise ballast maintenance cycle.

2. Methodology

In this research, machine learning (ML) models are used to investigate the suitability of incorporating CR particles among ballast extracted from non-identical parent rocks on the degradation resistance. Ballast samples have been collected from five quarries and include rock types of trachyte, basalt, limestone, andesite, and marlstone. The developed large-scale impact loading test is conducted on different gradations of freshly crushed ballast reinforced with various fractions of CR particles, applying distinct stress levels to specify the degradation extent. Therefore, through the experimental program, variables including rock type, gradation of fresh ballast, stress level, and CR content are considered.

In the second stage, ML models, including random forest (RF) and support vector regression (SVR), are used to reveal the importance of these aforementioned variables. According to the sequential divisions of the current study illustrated in Fig. 1, diverse conditions of impact loading tests are established on rubberized ballast specimens, which are succinctly clarified in the following subsections.

2.1. Test material and equipment

2.1.1. Materials

2.1.1.1. Fresh crushed ballast. The properties of ballast particles derived from distinct parent rocks are summarized in Table 1. Taking into account the sieve size range of specimens gathered from various quarries, as well as the characterized gradation curves from previous studies [43] depicted in Fig. 2, five distinct gradations of granular specimens were selected which fulfil the AREMA recommendations. Table 2 abridges the main characteristics corresponding to the selected gradations of fresh ballast particles.

2.1.1.2. Crumb rubber particles. The CR materials were derived from end-of-life bicycle tires by granulating and disintegrating large-sized particles. The specific gravity of the prepared rubber material is

a Impact loading test apparatus

b Load cell for determination of impact force

c Ballast specimen inside the main mold (0% CR)

d Overhead plate

Fig. 4. Large-scale impact loading test apparatus used for exerting impact loads on the ballast.

approximately 1.10. The characterized size range of CR particles is between 9.5 and 25 mm. In this regard, Khoshoei et al. [24] reported that the stiffness of specimens with larger-derived aggregate (20–60 mm) was significantly less than that of rubber granules in the range of 10 to 20 mm. Also, as pointed out by Arachchige et al. [4], the merit of establishing a CR size range from 9.5 to 19 mm was associated with a decrease in the breakage of large-sized particles. Moreover, the incorporation of rubber particles smaller than 9.5 mm could hinder the drainage of water, especially in the case of contamination due to the invasion of exterior small-sized particles. Furthermore, considering previous relevant studies [39,26], volume-based quotas of 0 %, 5 %, 10 %, 20 %, and 30 % were established to reinforce the crushed ballast with a characterized by-product. Fig. 3 illustrates the fresh ballast and CR particles, as well as the ballast-CR mixtures representing the rock-based ballast from different quarries.

2.1.2. Large-scale impact loading test

To assess the degradation resistance of ballast particles under impact loading, the ballast samples are subjected to a developed large-scale drop-weight impact loading test, which represents a simple index test for the assessment of ballast quality. The impact loading device was assembled based on the European standard [10], taking into account the actual loading extent exerted on the ballast layer in the field.

Fig. 4a illustrates the impact loading testing device, which includes a specimen mold (with a diameter of 240 mm) and a hammer (weighing 50 kg) used to apply falling-weight induced impact loading. Fig. 4b shows the position of the compression load cell used to measure the impact force applied to the ballast specimen. By adjusting the falling height, different stress magnitudes are applied to the prepared sample. Fig. 5 illustrates the stress levels applied, which comply well with the range of stress levels recommended by AREMA [5] for the ballast layer. The measured values represent the utmost impact force applied to a

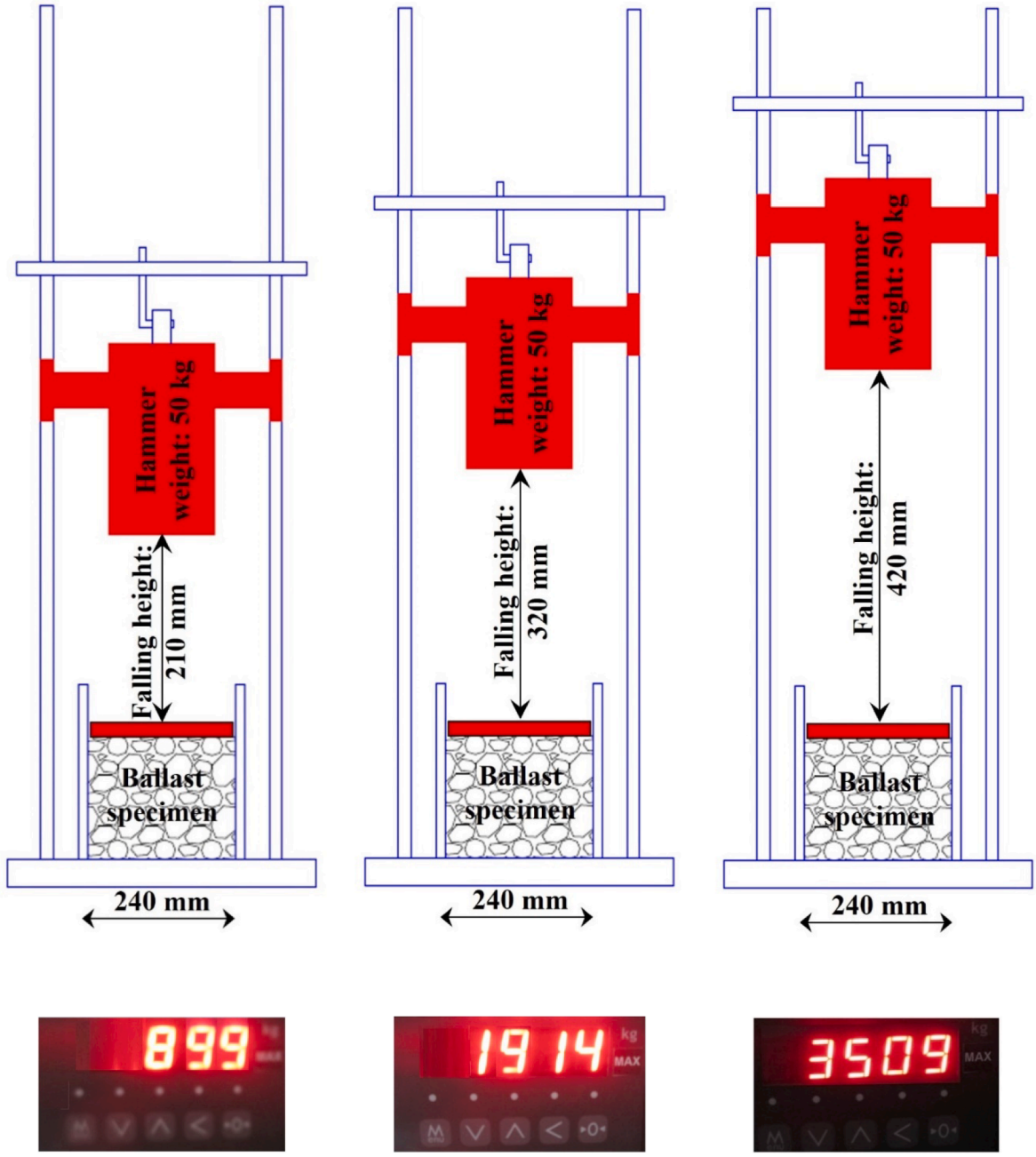

Fig. 5. Established falling height through the impact loading test for implementing the characterized stress levels on prepared specimens of the ballast-rubber mixture.

prepared specimen comprising only ballast particles. As expected, reinforcing the ballast particles with crumb rubber particles eventuates in an abatement in stress magnitude.

For each specified condition, 40 shocks are applied to the ballast specimens via impact loading, whether incorporating various percentages of CR or not, by adjusting the predetermined falling height levels. After this, the degraded ballast sample is sieved to specify the extent of degradation. In this regard, Qian et al. [34] considered the effect of the number of drum turns on changes in the size of ballast during the LAA. Likewise, as reported by Alves and Gomes [3], additional weathering cycles lead to more particle breakdown and disaggregation through physical and chemical weathering cycles. Similarly, in this study, the application of a higher number of blows leads to additional disintegration of the specimen.

2.1.3. Quantification of ballast degradation

To appraise the level of deterioration, two diverse degradation indices are computed as follows:

1. Fouling index (FI): The value of FI is quantified by the Eq. (1) as defined by Selig and Waters [38]

$$FI = P_4 + P_{200} \quad (1)$$

P_4 = Percentage of particles passing through 4.75 mm sieve
P_{200} = Percentage of particles passing through 0.075 mm sieve.

Fig. 6. Comparing the gradation of rubberized ballast specimens derived from distinct parent rock types before and after impact loading.

2. Marsal's breakage ratio (B_g): Quantification of breakage ratio by adding up the positive values of the difference in percentage retained on the same sieve size after the impact test. The variation in percentage remained on each sieve size (ΔW_k) is calculated as follows [32]:

$$\Delta W_k = W_{ki} - W_{kf} \quad (2)$$

W_{ki} = The percentage retained on sieve size k before the impact test
W_{kf} = The percentage retained on sieve size k after the impact test.

Fig. 6 demonstrates the intact ballast-CR specimens prepared for impact loading test upon which the degraded samples are generated, as shown for three parent rock types.

2.2. Machine learning models

2.2.1. Random forest model

Random forest (RF) regression is explicated as a supervised learning approach, where a composite of multiple machine learning procedures is established to enhance prediction truthfulness, identified as an ensemble procedure [28,21]. As schematically illustrated in Fig. 7, multiple regression trees are established to run in parallel, thereby reducing the variance of the learning approach [20].

In this procedure, the training data are initially split into several subdivisions by intermittently sampling the data for separate training,

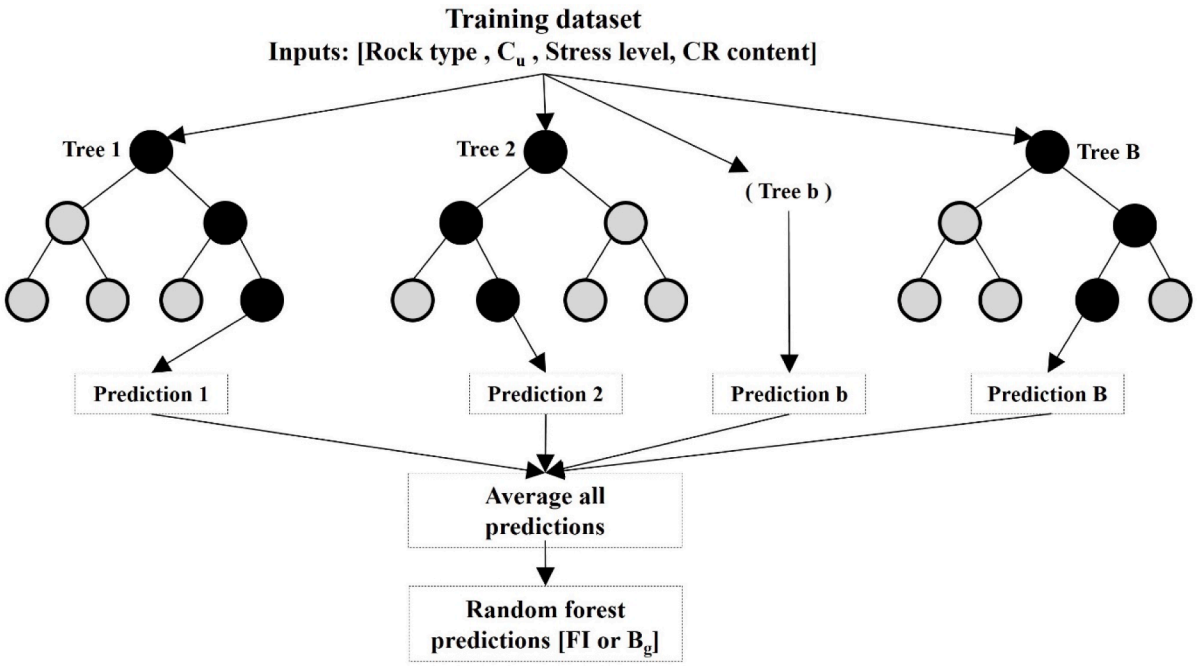

Fig. 7. A representative arrangement of RF regression structure.

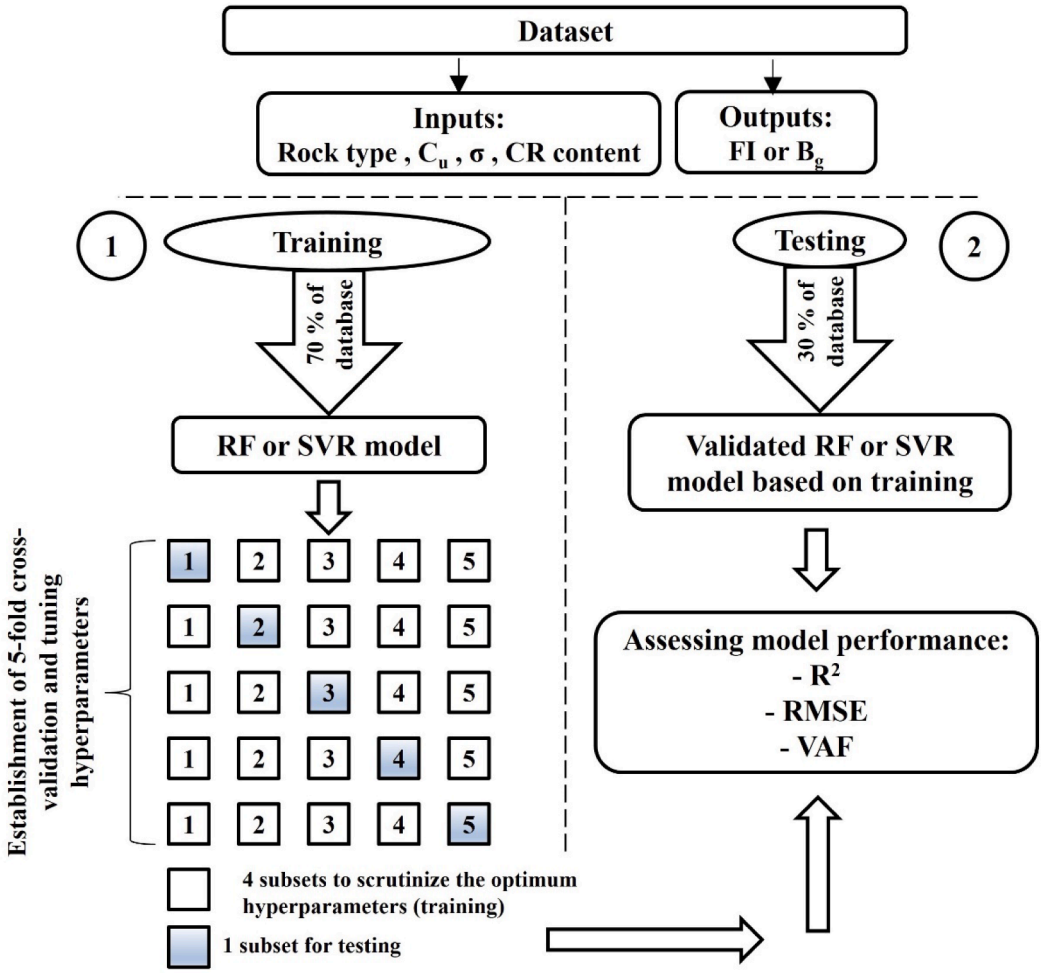

Fig. 8. Schematic layout of established approach for training and testing the ML models.

Table 3
Average values of computed degradation indices for different characterized conditions of parent rock type, gradation of fresh ballast, applied stress level and CR percentage.

Parent rock type	CR content (%)					CR content (%)				
	0	5	10	20	30	0	5	10	20	30
	Gradation of ballast: AREMA No. 3					Gradation of ballast: AREMA No. 4				
	Stress level: 200 kPa									
Trachyte	2.1 [1] / 10.8	1.7 / 9.3	1.4 / 8.9	1.2 / 8.5	1.1 / 8.3	2.5 / 12.6	2.1 / 10.9	1.7 / 9.4	1.4 / 9.0	1.2 / 8.7
Basalt	2.4 / 13.4	2.0 / 11.7	1.9 / 11.0	1.7 / 9.8	1.6 / 9.2	2.8 / 14.4	2.3 / 12.6	2.1 / 11.9	1.9 / 11.2	1.8 / 10.7
Limestone	3.3 / 16.2	2.6 / 14.2	2.3 / 12.6	2.0 / 11.3	1.8 / 10.6	3.6 / 17.5	3.0 / 15.3	2.6 / 14.1	2.3 / 12.8	2.1 / 11.6
Andesite	5.6 / 25.8	4.6 / 22.3	4.1 / 20.1	3.7 / 18.3	3.5 / 17.6	6.1 / 28.3	5.2 / 24.5	4.3 / 21.6	4.0 / 20.3	3.7 / 19.2
Marlstone	8.3 / 33.5	6.1 / 26.8	5.0 / 24.6	4.3 / 22.4	4.0 / 21.4	9.6 / 35.0	7.2 / 28.5	5.5 / 26.2	4.4 / 24.5	4.1 / 23.1
	Stress level: 420 kPa									
Trachyte	3.2 / 20.2	2.4 / 16.3	2.0 / 13.9	1.5 / 11.3	1.4 / 10.2	3.7 / 21.5	3.1 / 16.9	2.5 / 14.8	1.9 / 12.3	1.5 / 10.9
Basalt	3.6 / 22.4	2.8 / 18.1	2.4 / 15.3	2.0 / 12.7	1.8 / 11.5	4.3 / 23.5	3.0 / 18.9	2.5 / 16.3	2.1 / 13.7	1.8 / 12.6
Limestone	6.4 / 24.1	5.2 / 19.3	4.7 / 17.0	4.2 / 14.4	4.0 / 12.4	6.9 / 25.9	5.8 / 20.2	5.2 / 17.9	4.7 / 15.3	4.4 / 13.5
Andesite	8.2 / 31.1	6.8 / 27.1	6.2 / 25.9	5.6 / 24.7	5.4 / 24.2	8.9 / 39.2	7.6 / 35.6	7.0 / 33.3	6.3 / 32.1	5.9 / 30.9
Marlstone	12.1 / 42.4	10.9 / 39.0	10.2 / 36.9	9.3 / 35.5	9.1 / 34.6	12.6 / 43.3	11.4 / 39.9	10.6 / 38.1	10.1 / 36.7	9.6 / 35.7
	Stress level: 780 kPa									
Trachyte	5.2 / 29.0	3.8 / 19.9	2.8 / 16.3	2.1 / 14.0	1.9 / 13.4	5.7 / 29.9	4.2 / 21.0	3.2 / 17.4	2.5 / 15.2	2.1 / 14.1
Basalt	5.9 / 30.0	4.3 / 22.0	3.4 / 17.4	3.0 / 15.2	2.7 / 14.0	6.7 / 31.2	5.0 / 22.9	3.9 / 19.0	3.3 / 16.3	3.0 / 14.9
Limestone	9.0 / 32.0	7.9 / 26.5	7.4 / 23.3	7.0 / 21.3	6.6 / 20.0	9.9 / 33.5	8.6 / 28.1	8.1 / 24.5	7.4 / 22.1	7.1 / 21.1
Andesite	12.1 / 37.3	11.6 / 35.2	11.1 / 33.4	10.6 / 31.8	10.4 / 31.0	13.0 / 38.9	12.3 / 36.1	11.8 / 34.4	11.4 / 32.9	11.2 / 30.7
Marlstone	14.8 / 48.3	14.2 / 46.7	13.8 / 45.3	13.5 / 44.0	13.4 / 43.2	15.7 / 49.9	14.6 / 48.6	14.0 / 47.3	13.8 / 45.9	13.6 / 44.3
	Gradation of ballast: AREMA No. 4A					Gradation of ballast: AREMA No. 24				
	Stress level: 200 kPa									
Trachyte	1.7 / 9.6	1.3 / 8.2	1.1 / 8.0	0.9 / 7.9	0.8 / 7.8	2.0 / 10.5	1.9 / 9.0	1.3 / 8.6	1.1 / 8.2	1.0 / 8.0
Basalt	2.0 / 12.1	1.6 / 10.6	1.4 / 10.0	1.2 / 9.0	1.1 / 8.5	2.3 / 13.2	1.9 / 11.4	1.8 / 10.7	1.6 / 9.6	1.5 / 9.0
Limestone	2.9 / 14.5	2.2 / 12.9	1.9 / 11.6	1.7 / 10.2	1.6 / 9.8	3.2 / 15.9	2.5 / 13.8	2.2 / 12.3	1.9 / 11.0	1.7 / 10.4
Andesite	5.0 / 24.1	3.9 / 20.3	3.4 / 18.6	2.9 / 17.2	2.7 / 16.6	5.5 / 25.3	4.5 / 21.9	4.0 / 19.7	3.6 / 18.0	3.4 / 17.3
Marlstone	7.3 / 32.0	5.4 / 24.3	4.4 / 22.9	3.8 / 21.0	3.4 / 20.1	8.1 / 33.0	5.9 / 26.0	4.8 / 24.0	4.2 / 22.0	3.9 / 21.0
	Stress level: 420 kPa									
Trachyte	2.7 / 18.5	2.0 / 14.0	1.7 / 12.1	1.2 / 10.2	1.0 / 9.5	3.1 / 19.8	2.3 / 15.9	1.9 / 13.5	1.4 / 10.9	1.3 / 9.8
Basalt	3.1 / 20.3	2.5 / 16.3	2.1 / 13.4	1.7 / 11.4	1.5 / 10.5	3.5 / 21.9	2.7 / 17.6	2.3 / 14.9	1.9 / 12.4	1.7 / 11.1
Limestone	5.8 / 22.6	4.7 / 18.1	4.3 / 15.2	3.8 / 12.8	3.5 / 11.3	6.2 / 23.7	5.0 / 18.9	4.6 / 16.6	4.1 / 13.9	3.9 / 12.1
Andesite	7.5 / 29.8	6.2 / 26.1	5.7 / 24.7	5.2 / 23.4	4.9 / 22.7	7.8 / 30.6	6.6 / 26.7	6.0 / 25.4	5.5 / 24.3	5.3 / 23.7
Marlstone	11.0 / 40.3	9.9 / 37.6	9.2 / 35.4	8.6 / 34.2	8.3 / 32.9	11.9 / 42.0	10.7 / 38.6	10.0 / 36.6	9.4 / 35.2	9.0 / 34.3
	Stress level: 780 kPa									
Trachyte	4.8 / 28.0	3.4 / 19.0	2.4 / 15.1	1.7 / 12.9	1.5 / 11.3	5.0 / 28.6	3.6 / 19.6	2.6 / 15.9	1.9 / 13.7	1.7 / 12.9
Basalt	5.5 / 29.0	3.8 / 21.1	3.0 / 16.5	2.6 / 14.2	2.3 / 12.9	5.7 / 29.7	4.0 / 21.7	3.2 / 17.2	2.8 / 14.9	2.6 / 13.7
Limestone	8.5 / 30.5	7.6 / 25.0	7.0 / 21.6	6.7 / 20.2	6.5 / 19.5	8.9 / 31.7	7.8 / 26.2	7.3 / 22.9	6.9 / 20.9	6.5 / 19.7
Andesite	11.5 / 35.0	11.0 / 33.2	10.7 / 31.9	10.3 / 30.9	10.1 / 30.1	11.9 / 37.0	11.4 / 34.9	11.0 / 32.9	10.5 / 31.4	10.3 / 30.7
Marlstone	14.0 / 46.9	13.8 / 45.5	13.5 / 43.9	13.1 / 42.7	12.8 / 41.9	14.5 / 47.8	13.9 / 46.2	13.6 / 44.9	13.3 / 43.6	13.2 / 42.8
	Gradation of ballast: AREMA No. 25									
	Stress level: 200 kPa					Stress level: 420 kPa				
Trachyte	1.3 / 8.5	1.0 / 7.4	0.8 / 7.1	0.6 / 6.9	0.5 / 6.8	2.4 / 16.7	1.7 / 12.9	1.4 / 11.3	1.1 / 9.4	0.9 / 9.3
Basalt	1.6 / 11.0	1.3 / 9.7	1.1 / 9.0	0.9 / 8.4	0.8 / 8.2	2.7 / 18.7	2.1 / 14.9	1.9 / 12.7	1.4 / 10.9	1.3 / 10.2
Limestone	2.5 / 13.3	1.9 / 11.8	1.6 / 10.9	1.5 / 9.7	1.4 / 9.4	5.2 / 20.9	4.4 / 17.0	3.9 / 14.3	3.6 / 11.8	3.4 / 11.5
Andesite	4.4 / 22.7	3.6 / 19.1	3.2 / 17.7	2.7 / 16.4	2.5 / 15.9	6.9 / 26.8	5.8 / 24.2	5.4 / 22.8	5.0 / 21.6	4.7 / 21.3

(*continued on next page*)

Table 3 (*continued*)

Parent rock type	CR content (%)					CR content (%)				
	0	5	10	20	30	0	5	10	20	30
	Gradation of ballast: AREMA No. 3					Gradation of ballast: AREMA No. 4				
	Stress level: 200 kPa									
Marlstone	6.7 / 31.6	4.8 / 25.5	4.0 / 22.9	3.5 / 21.0	3.1 / 20.1	10.3 / 38.6	9.3 / 36.2	8.7 / 34.5	8.3 / 32.8	8.1 / 31.7
	Stress level: 780 kPa									
	CR content (%): 0		CR content (%): 5		CR content (%): 10		CR content (%): 20		CR content (%): 30	
Trachyte	4.2 / 25.7		2.8 / 17.6		2.0 / 14.1		1.4 / 11.3		1.2 / 10.9	
Basalt	5.0 / 26.9		3.5 / 19.6		2.8 / 15.2		2.3 / 13.6		2.1 / 12.7	
Limestone	7.8 / 28.2		7.1 / 22.7		6.6 / 19.4		6.2 / 17.5		5.9 / 17.2	
Andesite	10.9 / 32.6		10.4 / 30.7		10.0 / 29.6		9.7 / 28.6		9.5 / 27.9	
Marlstone	13.3 / 43.9		13.1 / 42.7		12.8 / 42.2		12.7 / 41.3		12.6 / 40.5	

[1] $\frac{FI}{B_g}$.

Table 4
Performance indices computed for training and testing datasets based on the characterized ML models.

ML model	Degradation index	Training			Testing		
		R^2	RMSE (%)	VAF (%)	R^2	RMSE (%)	VAF (%)
RF	FI	0.999	0.141	99.934	0.992	0.324	99.684
	B_g	0.998	0.419	99.928	0.988	1.145	99.551
SVR	FI	0.989	0.393	99.454	0.981	0.678	98.461
	B_g	0.977	1.608	98.823	0.959	2.367	98.296

We declare that we do not have any commercial or associative interest that represents a conflict of interest in connection with the work submitted.

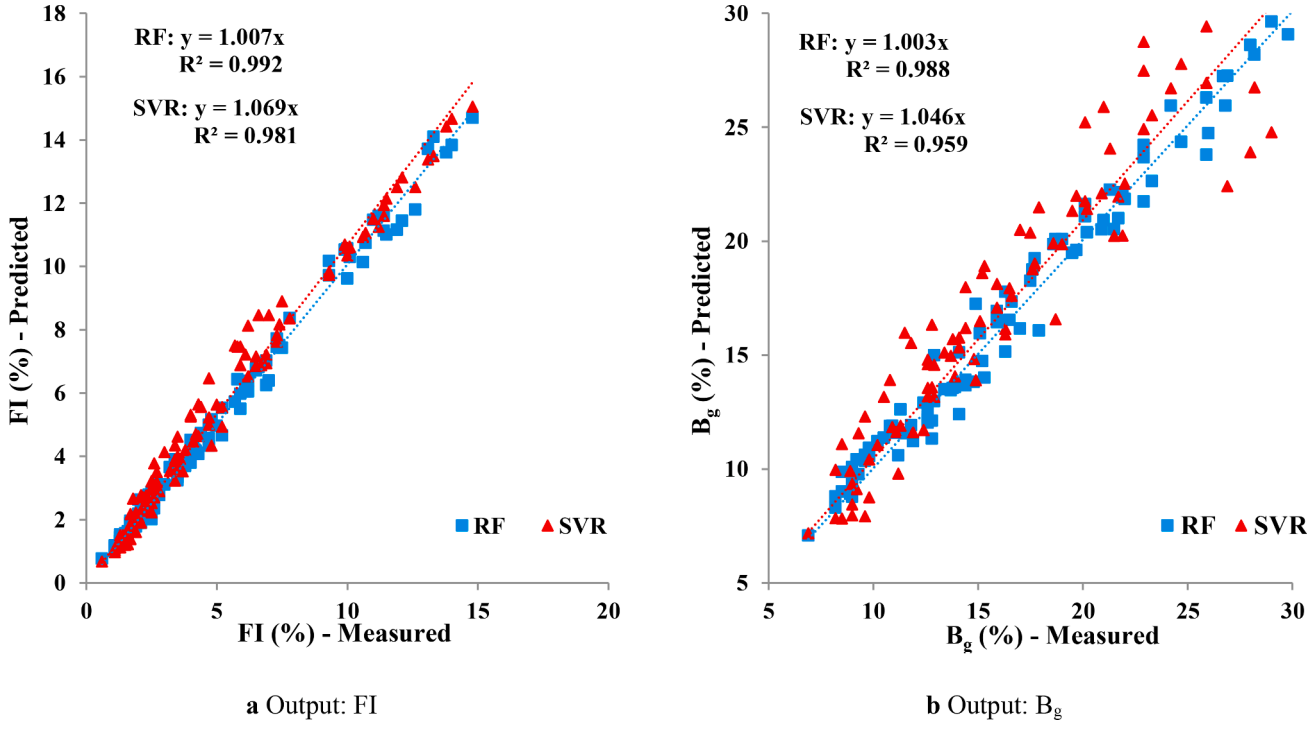

Fig. 9. Measured versus predicted values of target features based on the utilized ML models.

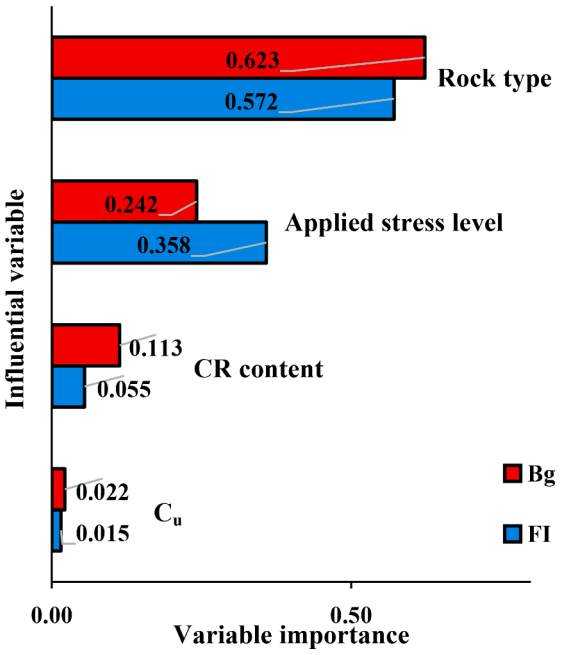

Fig. 10. Contribution of considered inputs on estimated values of FI and B_g - Based on the RF model.

referred to as bootstrapping. In this step, subsets of data and features are selected from the prepared dataset to construct each individual regression tree. Subsequently, the final output is estimated by integrating and averaging the outcomes of all trees, a process known as aggregation.

$$\widehat{y} = \frac{1}{B}\sum_{b=1}^{B} f_b(x) \tag{3}$$

$\widehat{y}$ = Final output
$f_b(x)$ = bth bootstrapped regression tree.
B = Number of separate regression trees.

2.2.2. SVR model

Support vector regression (SVR) is a form of machine learning model where the main goal is to find a regression function that has a maximum deviation from the actual targets, representing an extremely flat hyperplane. To achieve this, the inputs are initially delineated to a high-dimensional feature space. Then, the regression function in the designated feature space is determined by identifying the least of the risk function. The regression function can be expressed as follows [44]:

$$\widehat{y} = f(x) = w.\varphi(x) + b \tag{4}$$

$f(x)$ = Regression function
w = Weight vector.
$\varphi(x)$ = Mapped input onto high-dimensional feature space.
b = Bias of the model.

Also, the risk function is represented as follows considering the characterized constraints of Eqs. (6) and (7):

$$\tau(w,\xi^+,\xi^-) = \frac{1}{2}|w|^2 + C.\frac{1}{n}\sum_{i=1}^{n}(\xi_i^- + \xi_i^+), \quad i = 1,2,\ldots,n \tag{5}$$

$$(w.\varphi(x) + b) - y_i \leqslant \varepsilon + \xi_i^-, \quad i = 1,2,\ldots,n \tag{6}$$

$$y_i - (w.\varphi(x) + b) \leqslant \varepsilon + \xi_i^+, \quad i = 1,2,\ldots,n \tag{7}$$

C = Regularization parameter.
ξ_i^- *and* ξ_i^+ = Slack variables.
ε = Vapnik's insensitive loss.

2.2.3. Implementing the ML models on data and performance assessment

A database of 360 specimens is prepared to train and test the machine learning models developed for evaluating the degradation level of the ballast-CR mixture. The output variable is the degradation resistance, quantified based on the defined indices, and the input variables are the parent rock type, the gradation of fresh ballast, the stress level applied through the impact loading test, and the CR content, respectively. In this study, following relevant studies [42,17,9], 70 % of the dataset is employed to train the model, while the remaining 30 % is used as the testing set.

The accuracy of machine learning models developed for predicting the characterized outputs based on the input variables is assessed by computing the following statistical indices [31,45]:

$$R^2 = \left[\frac{\sum_{i=1}^{n}(y_i - \mu_y)(\widehat{y}_i - \widehat{\mu}_y)}{\sqrt{\sum_{i=1}^{n}(y_i - \mu_y)^2 \sum_{i=1}^{n}(\widehat{y}_i - \widehat{\mu}_y)^2}}\right]^2 \tag{8}$$

$$RMSE = \sqrt{\sum_{i=1}^{n}(y_i - \widehat{y}_i)/n} \tag{9}$$

$$VAF = \left(1 - \frac{Var|y - \widehat{y}|}{Var(y)}\right) \times 100 \tag{10}$$

R^2 = Coefficient of determination
$RMSE$ = Root mean square error
VAF = Variance account for
y = Actual values of $y_1, y_2, \ldots, y_n$
$\widehat{y}$ = Predicted values of $\widehat{y}_1, \widehat{y}_2, \ldots, \widehat{y}_n$
$\mu_y = E(y)$ = Average value of y
$\widehat{\mu}_y = E(\widehat{y})$ = Average value of $\widehat{y}$

To train and test the machine learning models, a large dataset of input–output combinations is prepared by conducting an impact loading test in which different conditions related to the parent rock type, the ballast gradation, the applied stress level, and the CR content are provided. The defined functions are as follows:

$$FI = f(Rock\,type, C_u, \sigma, CR\,content) \tag{11}$$

$$B_g = f(Rock\,type, C_u, \sigma, CR\,content) \tag{12}$$

C_u = Coefficient of uniformity based on the gradation curve of fresh ballast
σ = Stress level applied through the impact loading test.

Fig. 8 schematically illustrates the outline of training and testing the constructed ML models.

3. Results and discussion

3.1. Summary results of experimental program

In this subsection, the summary results of the impact loading test conducted on ballast-CR specimens are provided. Table 3 succinctly presents the values of ballast degradation resulting from the drop-weight impact loading test, based on two indices, namely FI and B_g. As noted, the abridged experimental outcomes border various conditions, such as the parent rock, ballast gradation, the applied stress level, and the CR percentage.

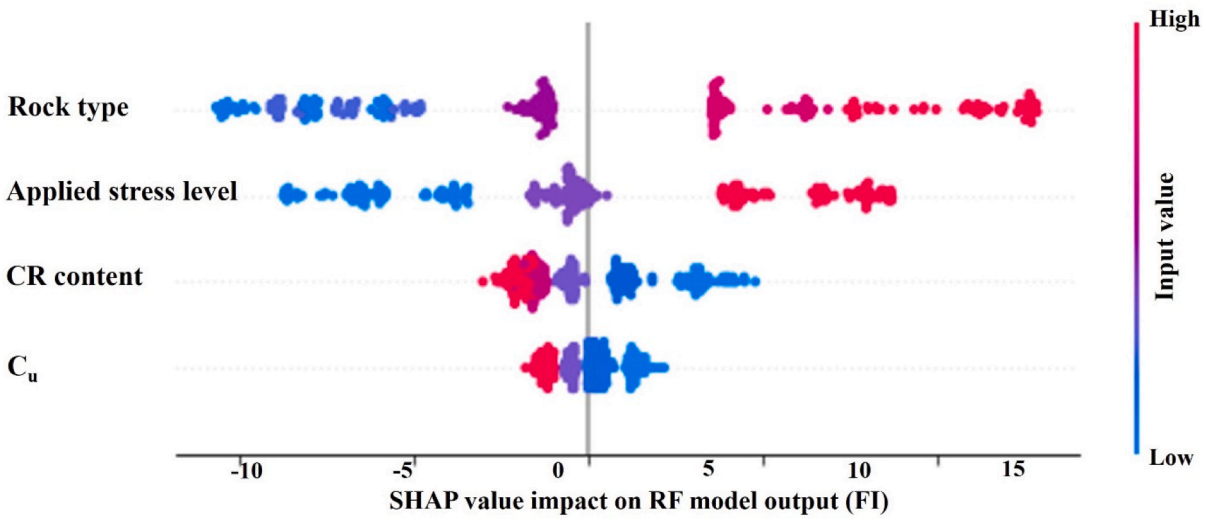

a Degradation index: FI

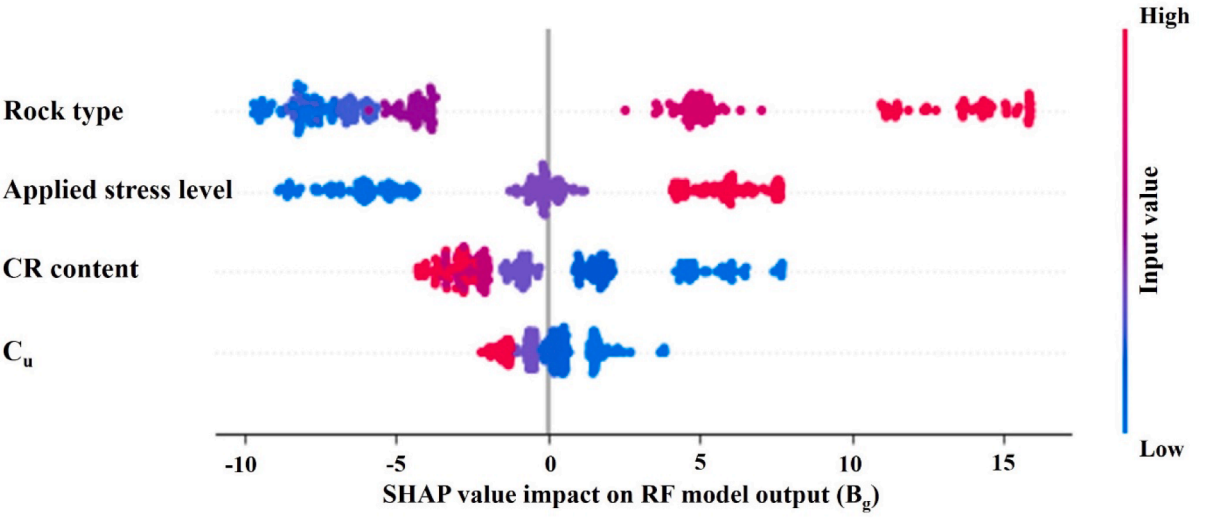

b Degradation index: B_g

Fig. 11. Summary plot of SHAP values of characterized inputs for each specific row of dataset based on the RF model - Red color representing the higher values of input, blue color representing lower values of input.

3.2. Summary results of ML models

3.2.1. Validation of models

In the present study, the hyperparameters of both ML models were tuned by employing a 5-fold cross-validation. In the case of RF regression, the number of trees in the forest (1–150), the maximum depth of the trees (2–16), and the minimum number of samples required to be at a leaf node (1–10) were examined to make out the optimum values. Implementation of the grid search method led to the determination of 100 trees, a maximum depth of 12, and a minimum sample leaf of 1. Similarly, in the case of SVR, tuning the RBF kernel parameters, including C (0.1–50) and gamma (0.01–10), was conducted using 5-fold cross-validation. Evaluation of the model performance for different combinations of these parameters' values based on the grid search method led to the optimal values of C = 10 and gamma = 0.1, representing the margin of the regression function and the inverse of the area of influence of the support vector, respectively.

Table 4 presents the derived values of computed indices representing the performance of developed predictive models based on the most appropriate parameters. Although the efficacy of both models is acceptable, the RF model outperforms the SVR. Similarly, Fig. 9 shows the measured degradation indices versus the predicted values of the characterized output features. The slope of the line with zero intercept further confirms the efficient predictive capability of both ML models.

3.2.2. Importance of characterized input variables

The contribution of the considered variables for mitigating the degradation of the ballast-CR mixture is evaluated by determining the factors of importance derived from validated ML models. As illustrated in Fig. 10 in an ascending pattern of significance, based on the RF regression characterized as the superior model, the most influential parameter is the parent rock type, followed by the applied stress level. Truly, the strength of the parent rock is a crucial property for an individual ballast particle to remain intact under impact loading.

The marginal influence of the gradation of fresh crushed ballast particles (based on C_u) on the degradation level of the ballast-rubber

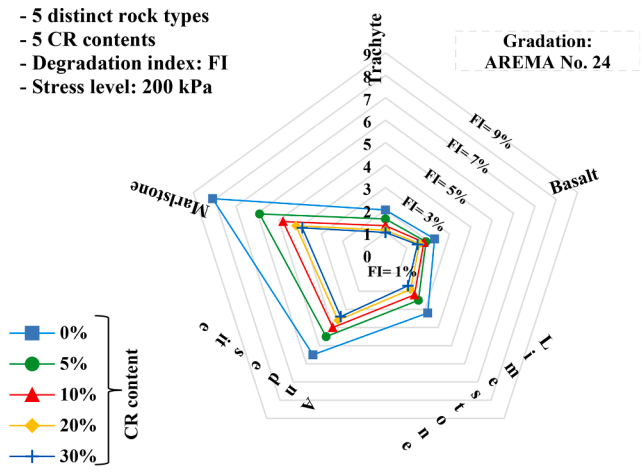

a.1 Stress level: 200 kPa

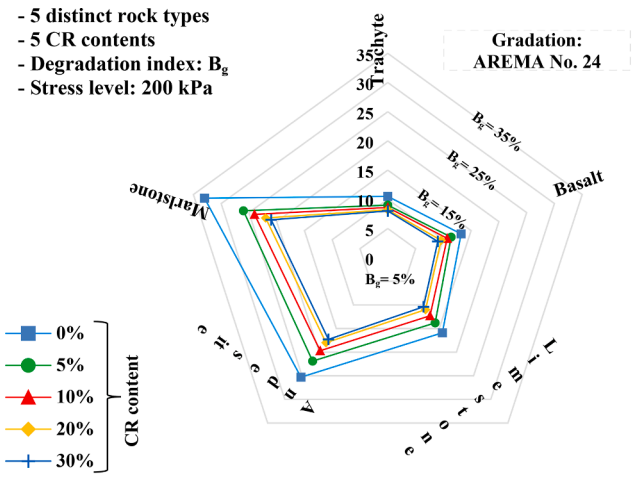

b.1 Stress level: 200 kPa

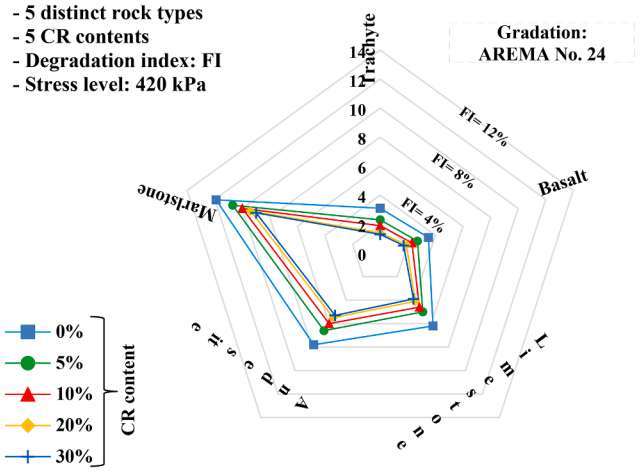

a.2 Stress level: 420 kPa

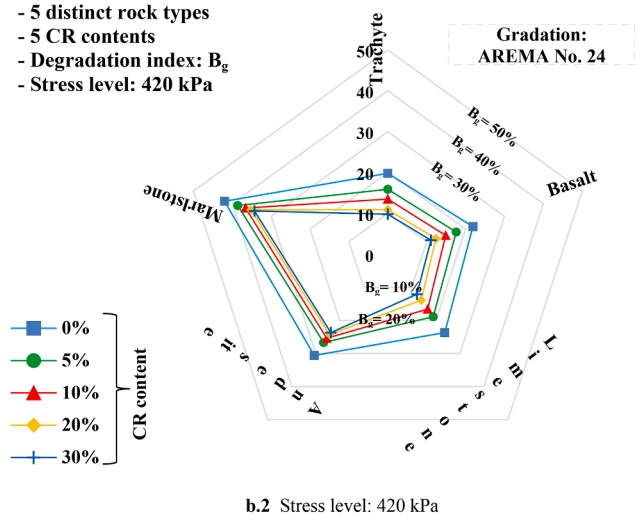

b.2 Stress level: 420 kPa

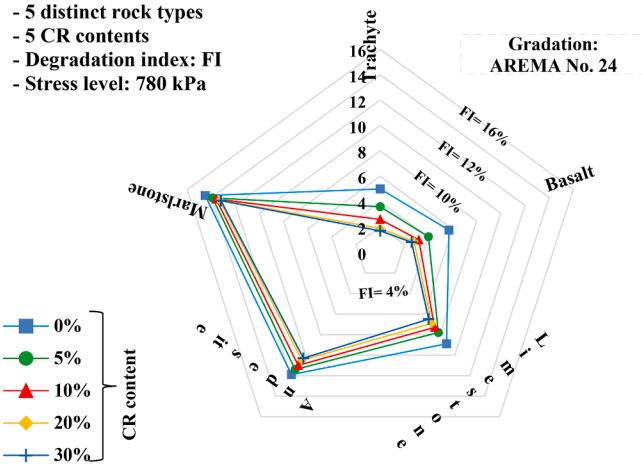

a.3 Stress level: 780 kPa

a Degradation index: FI

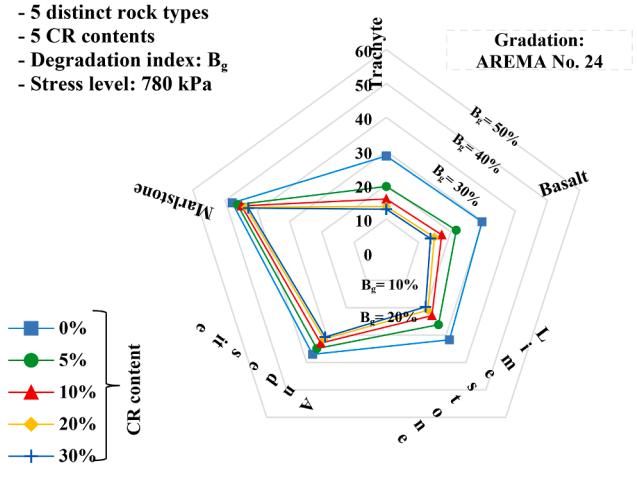

b.3 Stress level: 780 kPa

b Degradation index: B_g

Fig. 12. Effect of rock type and CR content on degradation level of ballast particles for distinct applied stress levels - Gradation of fresh ballast: AREMA No. 24.

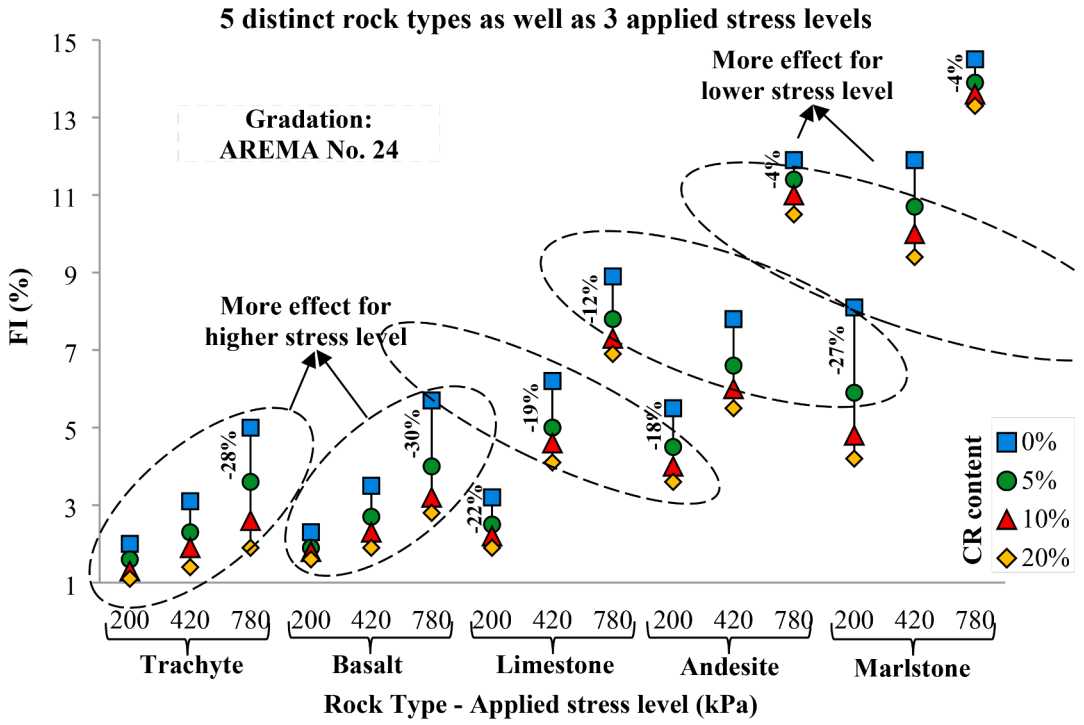

a Degradation index: FI

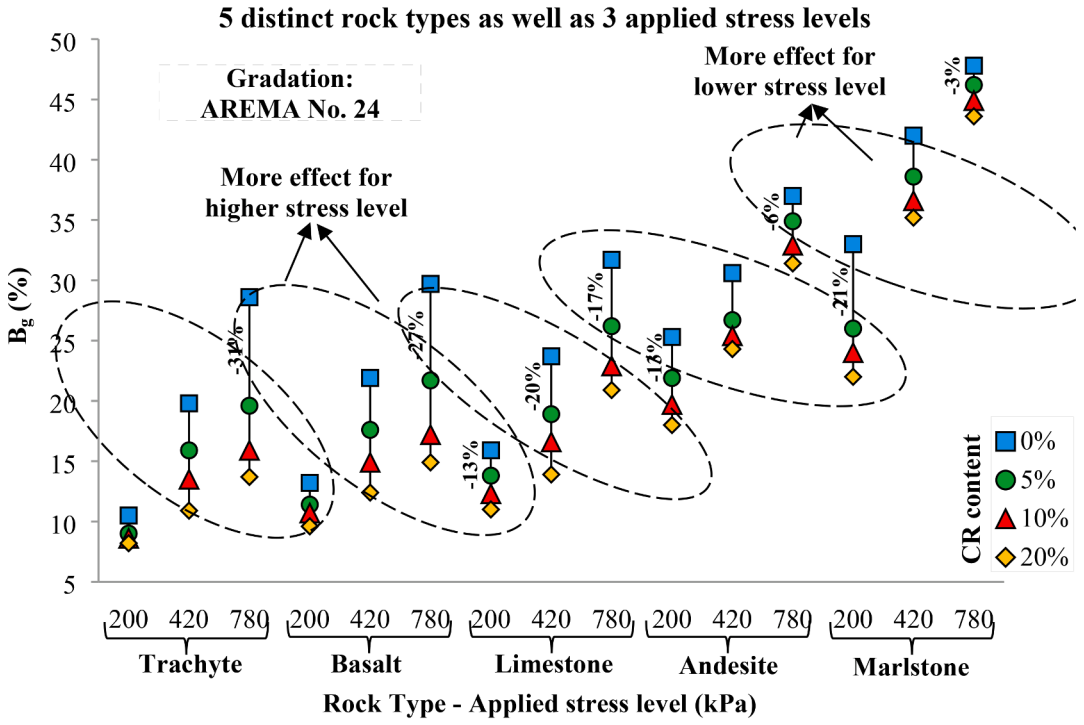

b Degradation index: B_g

Fig. 13. Effect of rock type and applied stress level on degradation level of ballast reinforced with CR particles - Gradation of fresh ballast: AREMA No. 24.

mixture can be attributed to the size range of the incorporated CR, i.e., 9.5–25 mm, leading to no meaningful difference between the large-sized gradations and the medium-sized ones. Meanwhile, Rosa et al. [36] observed more generation of fine particles passing through a 4.75 mm sieve after conducting a triaxial cyclic test when there was a further increment in the initial C_u values of ballast gradation.

Furthermore, the contribution of the rock type to the degradation index of B_g is higher than its influence on FI because the B_g index more significantly covers the breakage of individual particles instead of projection and abrasion of angular particles. Similarly, the effect of CR content on B_g is more evident because of the higher positive effect of rubber granules on bulk breakage rather than corner abrasion. In this regard, Zhang et al. [48] determined the same trend considering the degradation of ballast-CR samples exposed to impact loading.

The summary plot of Shapley values for each characterized input across the entire rows of the dataset is illustrated in Fig. 11. Each single point for an input variable represents the Shapley value of an individual row of the dataset, such that positioning on the right side of the x-axis confirms a direct influence of the characterized variable on the degradation level. Meanwhile, an indirect effect of a variable on FI or B_g is concluded whenever the single point is placed on the left side of the x-axis. For instance, change in the parent rock type from trachyte (1) to marlstone (5) leads to the variation of the dot's position from left (blue) to right (red), corroborating a surge in the degradation extent. Similarly, augmentation of the stress level from a lower value (blue) towards a higher value (red) results in a shift in the point position from left to right on the x-axis. On the contrary, an increase in the CR content and C_u brings about the reduction of both FI and B_g, although a subordinate influence is observed.

3.3. Discussion

3.3.1. Combined effect of rock type and CR content on degradation of ballast-rubber mixture

To understand the combined effectiveness of rock type and CR content on the degradation resistance of ballast particles, Fig. 12 is plotted solely for the initial gradation of AREMA No. 24 of fresh ballast. Truly, the outcomes of validated ML models affirm the marginal effect of the gradation of fresh crushed ballast.

Considering the depicted figure for each specific stress level, although an increase in CR percentage results in a reduction of FI and B_g indices, this influential effect is more noticeable in the case of using 5 % and 10 % rubber contents compared to the 0 % ballast-CR specimen. Afterwards, the incorporation of 20 % and 30 % of CR results in a reduction of degradation indices compared to specimens mixed with lower CR percent; however, this improvement is not significantly pronounced. Furthermore, as illustrated, the level of reduction of the characterized degradation indices caused by the addition of rubber material depends on the parent rock strength and the applied stress level through the impact loading test. This trend aligns well with the relative factors of importance derived through the validated ML models.

Generally, as expected, an increase in the amount of rubber particles contributes to mitigating ballast degradation. In this matter, Wu et al. [47] pointed out that the incorporation of waste tire-derived aggregate among ballast led to the reduction of contact stress. Likewise, the discrete element analysis of rubber-protected ballast subjected to cyclic loading and a direct shear test revealed a reduction of ballast-ballast contact and an augmentation of ballast-CR contact, leading to a surge in the coordination number and a decrease in the ballast breakage [14,49].

3.3.2. Combined effect of rock type and applied stress level on degradation of ballast-rubber mixture

Fig. 13 shows the variations of characterized degradation indices for distinct rock types and various implemented stress levels. Generally, the breakage of individual ballast particle is further exacerbated when high-level stress is applied or a low-strength parent rock is utilized. As illustrated, for lower stress levels (i.e. 200 kPa), the incorporation of rubber granules leads to a further abatement of degradation in the case of rock types with lower strength, like marlstone.

CR particles play an effective role in the plunge of degradation of high-strength rocks (trachyte and basalt) when high-stress levels (i.e. 780 kPa) are considered. This general trend is more pronounced for values of B_g, confirming further reduction of breakage of individual particle. Truly, a surge in the applied stress level results in considerable ballast breakage derived from weak parent rock so that no evident positive influence is observed through the incorporation of CR. Meanwhile, CR particles considerably improve the breakage resistance of rock types of trachyte and basalt subjected to the exacerbated stress level. Conversely, Esmaeili and Namaei [11] reported that rubber-coated ballast was more effective in the reduction of long-term settlement of ballast derived from parent rock with lower UCS. In this matter, Esmaeili et al. [12] pointed out that the effect of bedding modulus of under the sleeper pad was mitigated as long as the ballast material derived from the intact rock core with higher UCS was tested.

4. Conclusions

The present study investigated the influence of using granulated rubber in the ballast layer on degradation mitigation subjected to impact loading, considering the influences of parent rock strength along with the ballast gradation, the applied stress level, and the CR content. Particularly, machine-learning models, i.e., RF and SVR, were established to further reveal the involvement of aforementioned variables. Based on the observations of the current research, the following findings are relevant:

- The predictive performance of the RF model is superior to the SVR in order to anticipate the characterized degradation indices of the ballast-CR mixture.
- In order to mitigate the degradation level of ballast particles, the outcomes of validated ML models confirm that the parent rock type is the most influential parameter, followed by the applied stress level over the ballast specimen.
- The predictions of the RF model reveal that an increase in the C_u value of initial gradation of ballast constrains the FI and B_g, although the effect of this parameter is far less than other characterized factors.
- As expected, using a higher percentage of CR results in a more significant reduction of ballast degradation. Meanwhile, the most meaningful effect is achieved in the case of the incorporation of CR particles between 5 % and 10 %.
- Considering a low-stress level, the positive effect of CR on the diminution of degradation of particles is more highlighted in the case of ballast derived from low-strength parent rock (such as marlstone).
- In the case of high-strength parent rock (such as trachyte and basalt), CR granules are an influential additive to effectively suppress the degradation of ballast particles subjected to exacerbated stress levels.

CRediT authorship contribution statement

Mehdi Koohmishi: Writing – original draft, Visualization, Software, Methodology, Investigation, Data curation. **Yunlong Guo:** Writing – review & editing, Visualization, Supervision, Project administration, Methodology, Funding acquisition, Conceptualization.

Declaration of Competing Interest

The authors declare that they have no known competing financial interests or personal relationships that could have appeared to influence the work reported in this paper.

Data availability

Data will be made available on request.

Acknowledgements

The European Commission and UKRI Engineering and Physical Science Research Council (EPSRC) are acknowledged for the financial sponsorship of Re4Rail project (Grant No EP/Y015401/1).

References

[1] P. Aela, J. Wang, K. Yousefian, H. Fu, Z.Y. Yin, G. Jing, Prediction of crushed numbers and sizes of ballast particles after breakage using machine learning techniques, Constr. Build. Mater. 337 (2022), 127469.
[2] Y. Alabbasi, M. Hussein, Large-scale triaxial and box testing on railroad ballast: a review, SN Appl. Sci. 1 (12) (2019) 1592.
[3] H.C. Alves, G.J. Gomes, Weathering resistance of Linz-Donawitz (LD) slag as ballast material using freeze-thaw and sulfate soundness, Transp. Geotech. 40 (2023), 100973.
[4] C.M. Arachchige, B. Indraratna, Y. Qi, J.S. Vinod, C. Rujikiatkamjorn, Geotechnical characteristics of a rubber intermixed ballast system, Acta Geotech. 17 (5) (2022) 1847–1858.
[5] AREMA. (2010). Manual for railway engineering, Vol. 1: Track, Ch. 1: Roadway and Ballast. American Railroad Engineering and Maintenance of Way Association (AREMA), Washington, D.C.
[6] ASTM D 5731-02. (2002). Standard test method for determination of the point load strength index of rock. West Conshohocken, PA: American Society for Testing and Materials.
[7] ASTM C 535-03. (2003). Standard test method for resistance to degradation of large-size coarse aggregate by abrasion and impact in the Los Angeles machine. West Conshohocken, PA: American Society for Testing and Materials.
[8] ASTM C 127-12. (2012). Standard test method for density, relative density (specific gravity), and absorption of coarse aggregate. West Conshohocken, PA: American Society for Testing and Materials.
[9] M.J. Azarhoosh, M. Koohmishi, Prediction of hydraulic conductivity of porous granular media by establishment of random forest algorithm, Constr. Build. Mater. 366 (2023), 130065.
[10] EN 1097-2. (2010). European Standard: Tests for mechanical and physical properties of aggregates-Part 2: Methods for the determination of resistance to fragmentation. British Standard.
[11] M. Esmaeili, P. Namaei, Effect of mother rock strength on rubber-coated ballast (RCB) deterioration, Constr. Build. Mater. 316 (2022), 126106.
[12] M. Esmaeili, S. Farsi, A. Shamohammadi, Effect of rock strength on the degradation of ballast equipped with under sleeper pad, Constr. Build. Mater. 321 (2022), 126413.
[13] Y. Guo, V. Markine, W. Qiang, H. Zhang, G. Jing, Effects of crumb rubber size and percentage on degradation reduction of railway ballast, Constr. Build. Mater. 212 (2019) 210–224.
[14] Y. Guo, Y. Ji, Q. Zhou, V. Markine, G. Jing, Discrete element modelling of rubber protected ballast performance subjected to direct shear test and cyclic loading, Sustainability 12 (7) (2020) 2836.
[15] Y. Guo, J. Xie, Z. Fan, V. Markine, D.P. Connolly, G. Jing, Railway ballast material selection and evaluation: A review, Constr. Build. Mater. 344 (2022), 128218.
[16] Y. Guo, C. Shi, C. Zhao, V. Markine, G. Jing, Numerical analysis of train-track-subgrade dynamic performance with crumb rubber in ballast layer, Constr. Build. Mater. 336 (2022), 127559.
[17] L.S. Ho, V.Q. Tran, Machine learning approach for predicting and evaluating California bearing ratio of stabilized soil containing industrial waste, J. Clean. Prod. 370 (2022), 133587.
[18] B. Indraratna, W. Salim, C. Rujikiatkamjorn, Advanced rail geotechnology-ballasted track, CRC Press, 2011.
[19] B. Indraratna, D.J. Armaghani, A.G. Correia, H. Hunt, T. Ngo, Prediction of resilient modulus of ballast under cyclic loading using machine learning techniques, Transp. Geotech. 38 (2023), 100895.
[20] James, G., Witten, D., Hastie, T. and Tibshirani, R (2021). An introduction to statistical learning. 112, Second Edition, New York: Springer, 2021.
[21] S. Janitza, G. Tutz, A.L. Boulesteix, Random forest for ordinal responses: prediction and variable selection, Comput. Stat. Data Anal. 96 (2016) 57–73.
[22] X. Jiang, R. Xiao, Y. Bai, B. Huang, Y. Ma, Influence of waste glass powder as a supplementary cementitious material (SCM) on physical and mechanical properties of cement paste under high temperatures, J. Clean. Prod. 340 (2022) 130778.
[23] X. Jiang, Y. Zhang, Y. Zhang, J. Ma, R. Xiao, F. Guo, Y. Bai, B. Huang, Influence of size effect on the properties of slag and waste glass-based geopolymer paste, J. Clean. Prod. 383 (2023) 135428.
[24] S.M. Khoshoei, H. Mortazavi Bak, S. Mahdi Abtahi, S. Mahdi Hejazi, B. Shahbodagh, Experimental investigation of the cyclic behavior of steel-slag ballast mixed with tire-derived aggregate, J. Mater. Civ. Eng. 33 (2) (2021) 04020468.
[25] M. Koohmishi, M. Palassi, Evaluation of the strength of railway ballast using point load test for various size fractions and particle shapes, Rock Mech. Rock Eng. 49 (7) (2016) 2655–2664.
[26] M. Koohmishi, A. Azarhoosh, Degradation of crumb rubber modified railway ballast under impact loading considering aggregate gradation and rubber size, Can. Geotech. J. 58 (3) (2021) 398–410.
[27] M. Koohmishi, Assessing the strength of individual railway ballast aggregate by setting up bilateral point loading condition, Arab. J. Sci. Eng. 48 (4) (2023) 4393–4402.
[28] A. Liaw, M. Wiener, Classification and regression by random Forest, R News 2 (3) (2002) 18–22.
[29] J. Liu, F. Liu, C. Zheng, D. Zhou, L. Wang, Optimizing asphalt mix design through predicting the rut depth of asphalt pavement using machine learning, Constr. Build. Mater. 356 (2022), 129211.
[30] Z. Liu, B. Feng, E. Tutumluer, Effect of ballast degradation on track dynamic behavior using discrete element modeling, Transp. Res. Rec. 2676 (8) (2022) 452–462.
[31] S. Mangalathu, J.S. Jeon, Classification of failure mode and prediction of shear strength for reinforced concrete beam-column joints using machine learning techniques, Eng. Struct. 160 (2018) 85–94.
[32] R.J. Marsal, Large scale testing of rockfill materials, J. Soil Mech. Foundat. Division 93 (6) (1967) 383–388.
[33] C. Ngamkhanong, S. Kaewunruen, C. Baniotopoulos, Influences of ballast degradation on railway track buckling, Eng. Fail. Anal. 122 (2021), 105252.
[34] Y. Qian, H. Boler, M. Moaveni, E. Tutumluer, Y.M. Hashash, J. Ghaboussi, Degradation-related changes in ballast gradation and aggregate particle morphology, J. Geotech. Geoenviron. Eng. 143 (8) (2017) 04017032.
[35] G.P. Raymond, V.A. Diyaljee, Railroad ballast load ranking classification, J. Geotech. Eng. Div. 105 (10) (1979) 1133–1153.
[36] A.F. Rosa, F.T.S. Aragão, L.M.G. da Motta, Effects of particle size distribution and lithology on the resistance to breakage of ballast materials, Constr. Build. Mater. 267 (2021), 121015.
[37] J.M. Sadeghi, J.A. Zakeri, M. Najar, Developing track ballast characteristic guideline in order to evaluate its performance, Int. J. Railway 9 (2) (2016) 27–35.
[38] E.T. Selig, J.M. Waters, Track geotechnology and substructure management, Thomas Telford, London, 1994.
[39] M. Sol-Sánchez, N.H. Thom, F. Moreno-Navarro, M.C. Rubio-Gámez, G.D. Airey, A study into the use of crumb rubber in railway ballast, Constr. Build. Mater. 75 (2015) 19–24.
[40] M. Sol-Sánchez, F. Moreno-Navarro, G. Martínez-Montes, M.C. Rubio-Gámez, An alternative sustainable railway maintenance technique based on the use of rubber particles, J. Clean. Prod. 142 (2017) 3850–3858.
[41] M. Sol-Sánchez, F. Moreno-Navarro, R. Pérez, M.C. Rubio-Gámez, Defining the process of including sustainable rubber particles under sleepers to improve track behaviour and performance, J. Clean. Prod. 227 (2019) 178–188.
[42] M. Suthar, Applying several machine learning approaches for prediction of unconfined compressive strength of stabilized pond ashes, Neural Comput. & Applic. 32 (13) (2020) 9019–9028.
[43] Tutumluer, E., Huang, H., Hashash, Y.M.A., and Ghaboussi, J. (2009). AREMA gradations affecting ballast performance using discrete element modeling (DEM) approach. In Proceedings of the AREMA 2009 annual conference (pp. 20-23).
[44] V. Vapnik, The nature of statistical learning theory, second ed., Springer Science & Business Media, New York, 1999.
[45] T.G. Wakjira, M. Ibrahim, U. Ebead, M.S. Alam, Explainable machine learning model and reliability analysis for flexural capacity prediction of RC beams strengthened in flexure with FRCM, Eng. Struct. 255 (2022), 113903.
[46] M.A. Wnek, E. Tutumluer, M. Moaveni, E. Gehringer, Investigation of aggregate properties influencing railroad ballast performance, Transp. Res. Rec. 2374 (1) (2013) 180–189.
[47] H. Wu, L. Zhu, W. Song, Z. Xu, F. Xu, H. Gong, Impact performance of ballast by incorporating waste tire-derived aggregates, Constr. Build. Mater. 288 (2021), 122992.
[48] F. Zhang, J. Chang, H. Feng, Laboratory study on degradation of ballast mixed with crumb rubber under impact loads, Int. J. Rail Transp. (2022) 1–23.
[49] F. Zhang, Q. Yao, H. Wang, H. Feng, J. Chang, L. Lu, M. Jiang, DEM analysis of the cyclic behavior of ballast mixed with crumb rubber, Constr. Build. Mater. 375 (2023), 130975.
[50] C. Zhang, Z. Zhu, F. Liu, Y. Yang, Y. Wan, W. Huo, L. Yang, Efficient machine learning method for evaluating compressive strength of cement stabilized soft soil, Constr. Build. Mater. 392 (2023), 131887.